JOURNAL OF COMPUTATIONAL PHYSICS **138,** 103–120 (1997)
ARTICLE NO. CP975828

A 2D Analysis of the Influence of Artificial Viscosity Terms on Solutions of the Euler Equations

Gunilla Efraimsson[1]

C2M2, NADA, Royal Institute of Technology, S-100 44, Stockholm, Sweden
E-mail: gunillae@nada.kth.se

Received July 23, 1996; revised April 1, 1997

We analyze the influence of artificial viscosity on solutions of the Euler equations in the neighborhood of oblique shocks in 2D by studying a discrete, linear model equation. Based on the linear analysis an artificial viscosity model is derived. It is tested on two different test cases with the Euler equations: flow over a wedge and Mach-3 flow in a wind tunnel with a step.

1. INTRODUCTION

The purpose of this paper is to present a method on how to linearly analyze the influence of artificial viscosity on numerical solutions of the two-dimensional Euler equations when the solutions contain shocks. We consider central differences schemes where the artificial viscosity terms are added explicitly. Another, closely related, approach is flux vector splitting schemes, where the artificial viscosity is included in the numerical flux term.

In one dimension (1D), the amount of artificial viscosity needed to avoid oscillations has been analyzed by linear and nonlinear theory. See for instance [6, 9, 10, 14, 17]. The so-called TVD methods can be viewed as switching on a first-order artificial viscosity term with the use of a limiter function in the neighborhood of a discontinuity. Extensive work has been performed to further develop TVD methods [16, 20]. One-dimensional analysis is simplified by the physical fact that transportation of characteristic information is only possible in two directions. In higher dimensions, however, the number of flow directions are infinite. Goodman and LeVeque

[1] Present address: FFA, Box 11021, S-161 11 Bromma, Sweden. E-mail: eng@ffa.se.

0021-9991/97 $25.00

have shown that methods that are TVD in 2D, with the extension of the one-dimensional definitions of TVD to multidimensions, are at most first order accurate [8].

In two-dimensional calculations a straightforward approach is to extend the one-dimensional scheme in a dimensional splitting fashion. This approach is indeed easy to implement and, of course, produces satisfying results when the shock is aligned with the grid. However, too much artificial viscosity can be introduced by this approach and, thus, the results depend heavily on the behavior of the limiter. There is a wide flora of different limiters and their applications in calculations. Comprehensive numerical experiments have been performed in order to examine the behavior of the limiter functions in 2D; see e.g. [7, 19].

The drawback with the dimensional splitting approach has been pointed out by e.g. Davis, [4]. Davis developed a numerical method which used different formulas for the flux components normal and tangential to the shock direction.

Riemann solver-based schemes with different level of multidimensionality have been developed by, for instance, Deconinck, Hirsch, and Peuteman [5], LeVeque [11], Levy, Powell, and van Leer [12], and Roe [15]. Multidimensional ENO schemes have been derived by, for instance, Casper and Atkins [2].

In this paper we argue that the solution of a particular scalar discrete model equation is influenced by artificial viscosity terms in the same way as stationary solutions of the 2D Euler equations in the neighborhood of an oblique shock. Numerical experiments support this claim. In the analysis we only consider oblique shocks. However, locally also curved shocks can be considered as oblique. The model equation can be solved analytically for special values of the shock angle. A suitable artificial viscosity model for the linear model problem is obtained as a solution of an optimization problem. We use the results from the linear analysis in computations with the Euler equations in 2D for two different geometries: flow over a wedge and a Mach-3 flow in a wind tunnel with a step.

The paper is organized as follows: Section 2 contains the preliminaries with the presentation of the two-dimensional Euler equations and some well-known gas dynamic relations across an oblique shock. In Section 3 we motivate why a certain scalar equation models the behavior of the numerical solution of the full Euler equations in the neighborhood of an oblique shock. Also, we solve the model equation analytically for a special shock angle. Section 4 is devoted to numerical results, where we compare the analytical solution of the model equation and the numerical solution of the full two-dimensional Euler equations. From the model equation we also derive a numerical viscosity term and examine its behavior on two different test problems. In Section 5 we make conclusions and final remarks.

2. THE EULER EQUATIONS IN 2D

The Euler equations in 2D Cartesian coordinates in conservative variables are

$$\mathbf{u}_t + \mathbf{f}(\mathbf{u})_x + \mathbf{g}(\mathbf{u})_y = 0, \tag{1}$$

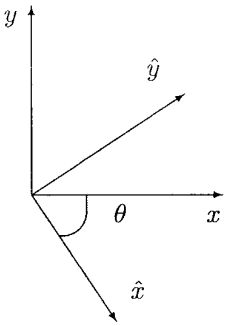

FIG. 1. Rotated system of reference.

where

$$\mathbf{u} = \begin{pmatrix} r \\ ru \\ rv \\ rE \end{pmatrix}, \quad \mathbf{f}(\mathbf{u}) = \begin{pmatrix} ru \\ (ru)^2/r + p \\ (ru)(rv)/r \\ ru(rE + p)/r \end{pmatrix}, \quad \mathbf{g}(\mathbf{u}) = \begin{pmatrix} rv \\ (ru)(rv)/r \\ (rv)^2/r + p \\ rv(rE + p)/r \end{pmatrix}. \tag{2}$$

Here, r is the density; ru and rv are the mass flux in the x- and y-directions, respectively; rE is the total energy. We consider calorically perfect gases, with the equation of state

$$p = (\gamma - 1)(rE - \frac{1}{2r}((ru)^2 + (rv)^2)).$$

The analysis in this paper is based on the rotation invariance property of the Euler equations. That is, consider the standard reference system (x, y), and a reference system $(\hat{x}, \hat{y})$ rotated by the angle θ (see Fig. 1). Due to rotational invariance it holds that the Euler equations in the rotated variables are

$$\hat{\mathbf{u}}_t + \mathbf{f}(\hat{\mathbf{u}})_{\hat{x}} + \mathbf{g}(\hat{\mathbf{u}})_{\hat{y}} = 0,$$

where

$$\hat{\mathbf{u}} = \begin{pmatrix} 1 & 0 & 0 & 0 \\ 0 & \cos\theta & \sin\theta & 0 \\ 0 & -\sin\theta & \cos\theta & 0 \\ 0 & 0 & 0 & 1 \end{pmatrix} \mathbf{u} := R\mathbf{u} \tag{3}$$

and $\mathbf{f}$ and $\mathbf{g}$ are similar as in Eq. (2).

In this paper we consider oblique shocks. The standard setup for an oblique shock is a supersonic flow over a wedge; a gas flows with supersonic speed toward

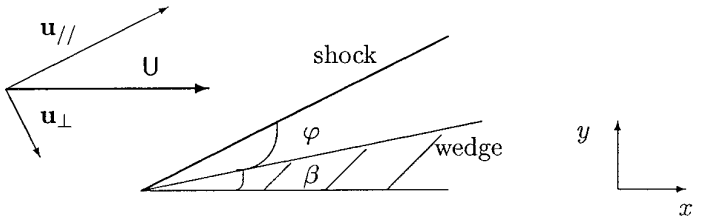

FIG. 2. Oblique shock in physical domain.

a wedge, with an angle β. An oblique shock will form, with an angle φ between the shock and the wedge (see Fig. 2).

There are some well-known gas dynamic relations for oblique shocks. Here we will recognize the following: Decompose the particle velocity field vector U into the components parallel, $\mathbf{u}_{/\!/}$, and normal, $\mathbf{u}_\perp$, to the shock, respectively. It can be shown that the length of the parallel velocity component, $u_{/\!/}$, is constant across an oblique shock, while the length of the normal velocity component, $u_\perp$, obeys one-dimensional shock theory. See, e.g. [1]. With the notation $u^{(1)}$ upstream of the shock, $u^{(2)}$ downstream, and c the speed of sound we have

$$u_{/\!/}^{(2)} = u_{/\!/}^{(1)}$$

$$u_\perp^{(2)} = h(M_\perp^{(1)}), \quad \text{where } M_\perp^{(1)} = \frac{u_\perp^{(1)}}{c^{(1)}}.$$

Here h is a function derived in one-dimensional analysis [1].

3. MODEL EQUATION

In this section we vindicate the use of a scalar difference equation as a model equation for the discretized Euler equations. The scalar equation can be solved analytically and the influence of artificial viscosity terms on the solution of the scalar problem can hence be studied. By comparing numerical results of the model and the Euler equations, respectively, we conclude that the model equation captures the most essential features of the solution of the slightly viscous Euler equations in the neighborhood of a shock wave.

To motivate why a scalar equation can model a system of equations we use the one-dimensional character of an oblique shock, that was mentioned in Section 2. From one-dimensional theory it is known that for weak shocks the quantity connected with the eigenvalue that changes sign across a shock will have a jump proportional to the shock strength (see [3]). The quantities connected with the other eigenvalues will have a jump proportional to the third power of the shock strength. For strong shocks the eigenvalues will be of approximately equal size, and we will see that it is sufficient to restrict the analysis to a scalar equation.

To begin with, we discretize and derive the linearized Euler equations. Thereafter we make use of the rotational invariance of the Euler equations and diagonalize

one part of the rotated system of the discrete equations. Finally, we find the scalar equation that serves as a model equation for a solution containing a 2D shock wave. The solution of the model equation for certain boundary conditions is presented in Lemma 5.

We discretize in space by letting $x_i = i\Delta x$ and $y_j = j\Delta y$, respectively. For simplicity, we let $\Delta x = \Delta y = h$. Also we introduce the grid functions

$$\mathbf{u}_{ij} \approx \mathbf{u}(x_i, y_j),$$

We approximate the derivatives with standard second-order accurate central differences. Near a shock, artificial viscosity terms must be added to achieve nonoscillatory solutions. Hence we consider

$$\mathbf{u}_t + D_0^x \mathbf{f}(\mathbf{u}_{ij}) + D_0^y \mathbf{g}(\mathbf{u}_{ij}) = D_+^x \varepsilon_{ij}^x D_-^x \mathbf{u}_{ij} + D_+^y \varepsilon_{ij}^y D_-^y \mathbf{u}_{ij}, \tag{4}$$

where

$$D_0^x u_{ij} = (u_{i+1,j} - u_{i-1,j})/2h, \quad D_+^x u_{ij} = (u_{i+1,j} - u_{i,j})/h, \quad D_-^x u_{i,j} = (u_{i,j} - u_{i-1,j})/h,$$

and correspondingly in the y-direction.

In the following analysis we study the steady sate solution downstream of an oblique shock. The corresponding analysis for the solution upstream of a shock is analogous. We consider the setup in Fig. 2. Make the ansatz

$$\mathbf{u}_{ij} = \mathbf{U} + \mathbf{u}'_{ij}, \quad \varepsilon_{ij}^x = \varepsilon^x + \varepsilon_{ij}^{x\prime}, \quad \varepsilon_{ij}^y = \varepsilon^y + \varepsilon_{ij}^{y\prime}, \tag{5}$$

where $\mathbf{U}$, ε^x, and ε^y are constant and the primed variables are small perturbations. With the ansatz (5) in Eq. (4) and linearizing by neglecting quadratic and higher order terms in $\mathbf{u}'$ and ε' we have

$$\mathbf{f}'(\mathbf{U}) D_0^x \mathbf{u}'_{ij} + \mathbf{g}'(\mathbf{U}) D_0^y \mathbf{u}'_{ij} = \varepsilon^x D_+^x D_-^x \mathbf{u}'_{ij} + \varepsilon^y D_+^y D_-^y \mathbf{u}'_{ij}, \tag{6}$$

where $f'(\mathbf{U}) = \partial \mathbf{f}/\partial \mathbf{u}(\mathbf{U})$ and analogously for $\mathbf{g}'(\mathbf{U})$. Recall that $\mathbf{U}$ is independent of i and j.

Multiplication with R, defined in Eq. (3), from the left yields

$$R\mathbf{f}'(\mathbf{U}) R^{-1} D_0^x R\mathbf{u}'_{ij} + R\mathbf{g}'(\mathbf{U}) R^{-1} D_0^y R\mathbf{u}'_{ij} = \varepsilon^x D_+^x D_-^x R\mathbf{u}'_{ij} + \varepsilon^y D_+^y D_-^y R\mathbf{u}'_{ij}. \tag{7}$$

We drop the primes and let

$$\hat{\mathbf{u}}_{ij} = R\mathbf{u}_{ij} = \begin{pmatrix} r \\ ru\cos\theta + rv\sin\theta \\ -ru\sin\theta + rv\cos\theta \\ rE \end{pmatrix}_{ij}, \quad \hat{\mathbf{U}} = R\mathbf{U}.$$

Due to the rotational invariance of the Euler equations we have

LEMMA 1.

$$R\mathbf{f}'(\mathbf{U})R^{-1} = a\mathbf{f}'(\hat{\mathbf{U}}) - b\mathbf{g}'(\hat{\mathbf{U}})$$
$$R\mathbf{g}'(\mathbf{U})R^{-1} = b\mathbf{f}'(\hat{\mathbf{U}}) + a\mathbf{g}'(\hat{U}),$$

where $a = \cos\theta$ and $b = \sin\theta$. The angle $\theta = \varphi - 90°$, where φ is the shock angle (see Fig. 2).

Proof. Straightforward calculations yield the lemma.

By Lemma 1 we see that Eq. (7) is equivalent with

$$\mathbf{f}'(\hat{\mathbf{U}})(aD_0^x\hat{\mathbf{u}}_{ij} + bD_0^y\hat{\mathbf{u}}_{ij}) + \mathbf{g}'(\hat{\mathbf{U}})(-bD_0^x\hat{\mathbf{u}}_{ij} + aD_0^y\hat{\mathbf{u}}_{ij}) = \varepsilon^x D_+^x D_-^x\hat{\mathbf{u}}_{ij} + \varepsilon^y D_+^y D_-^y\hat{\mathbf{u}}_{ij}. \tag{8}$$

The matrix $\mathbf{f}'(\hat{\mathbf{U}})$ can be diagonalized, since the Euler equations are hyperbolic. We let S and S^{-1} be matrices with the right eigen vectors of $\mathbf{f}'(\hat{\mathbf{U}})$ as columns and the left eigen vectors of $\mathbf{f}'(\hat{\mathbf{U}})$ as rows, respectively. Thus,

$$S^{-1}\mathbf{f}'(\hat{\mathbf{U}})S = \Lambda,$$

where $\Lambda = \mathrm{diag}(U_\perp, U_\perp, U_\perp + C, U_\perp - C)$. Multiplication by S^{-1} on Eq. (8) yields

$$\Lambda(aD_0^x + bD_0^y)\tilde{\mathbf{u}}_{ij} + G(-bD_0^x + aD_0^y)\,\tilde{\mathbf{u}}_{ij} = (\varepsilon^x D_+^x D_-^x + \varepsilon^y D_+^y D_-^y)\tilde{\mathbf{u}}_{ij}, \tag{9}$$

where

$$G = \begin{pmatrix} U_{//} & 0 & 0 & 0 \\ 0 & U_{//} & -C/2 & -C/2 \\ 0 & -C & U_{//} & 0 \\ 0 & -C & 0 & U_{//} \end{pmatrix}$$

and $\tilde{\mathbf{u}}_{ij} = S^{-1}\hat{\mathbf{u}}_{ij}$.

Equation (9) is still a coupled system of difference equations, since the matrix G is not diagonal. In the following, we argue that it is sufficient to study a solution of the form

$$\tilde{\mathbf{u}}_{ij} = \begin{pmatrix} 0 \\ 0 \\ 0 \\ \tilde{u}^{(4)} \end{pmatrix}_{i,j}. \tag{10}$$

As was mentioned at the end of Section 2, we know from continuous theory that for an oblique shock, the relations for changes across the shock are identical to the

one-dimensional results, although as functions of the normal component of the upstream Mach number, $M_{\perp,1}$. In other words, an oblique shock is equivalent to a one-dimensional shock when viewed in a reference system aligned with the shock.

At the beginning of this section we pointed out the one-dimensional result, that for a weak shock the jump in the quantity connected to the eigenvalue that changes sign across the shock is proportional to the shock strength, whereas the other quantities have a jump proportional to the third power of the shock strength. Let δ denote the shock strength. Since the eigenvalue $\lambda = u_\perp - c$ changes sign across a shock wave (see [13]), it follows that the continuous, linearized problem has boundary conditions at the shock of the form

$$\tilde{\mathbf{u}}|_{\text{shockboundary}} = \begin{pmatrix} \mathcal{O}(\delta^3) \\ \mathcal{O}(\delta^3) \\ \mathcal{O}(\delta^3) \\ \mathcal{O}(\delta) \end{pmatrix}.$$

Now consider the discrete, linearized problem, Eq. (9). In Eq. (9) the normal and tangential derivatives of the continuous problem are approximated with second-order accuracy in space. With the same type of boundary conditions as in the continuous case the quantity connected to $\lambda^{(4)}$ in the discretized equations, will be of $\mathcal{O}(\delta)$ at the shock boundary, whereas the quantities connected with the other eigenvalues are of order $\mathcal{O}(\delta^3)$. Since the coupling of the equations appears in the tangential derivative, which is $\mathcal{O}(h^2)$, the quantity connected to $\lambda^{(4)}$, is likely to be dominant throughout the computational domain. However, for a weak shock, $\lambda^{(4)} = U_\perp - C$ can be much smaller than $U_{//}$. Therefore, the term $\lambda^{(4)}(aD_0^x + bD_0^y)u_{i,j}^{(4)}$ can be of the same order as the term $U_{//}(-bD_0^x + aD_0^y)u_{i,j}^{(4)}$. Hence, both terms have to be considered in order to model the behavior close to a weak shock.

For strong shocks the diagonal part of (11) dominates for all components in $\tilde{\mathbf{u}}_{i,j}$. Also the eigenvalues are of approximately the same size. Therefore, a solution of the form (10) is sufficient also for strong shocks.

From the above discussion, we propose

Conjecture 1. *Consider the scalar equation*

$$(U_\perp - C)(aD_0^x + bD_0^y)u_{ij} + U_{//}(-bD_0^x + aD_0^y)u_{ij} = (\varepsilon^x D_+^x D_-^x + \varepsilon^y D_+^y D_-^y)u_{ij}. \quad (11)$$

with boundary conditions

$$u_{ij} = \mathcal{O}(1) \quad \textit{at the points that model the shock}$$
$$u_{i,j} \to 0, \qquad i \to \infty;\ \text{J} \to -\infty,$$

and the additional constraint

$u_{i,j}$ *is constant in the direction tangential to the shock.*

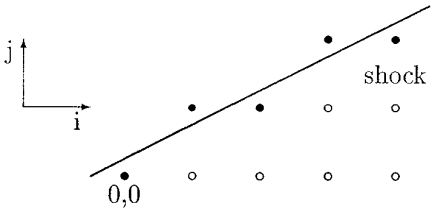

FIG. 3. Computational domain for the model equation (11) for the case $\tan \varphi = 0.5$. Black points (●) are discretization points that models the shock.

Also, consider the solution of the Euler equations, discretized as in (4), downstream of an oblique shock.

For all values of ε^x and ε^y, the solution of (11) and of the Euler equations are similar with respect to oscillations and smearing.

In Conjecture 1 we have replaced $\tilde{u}_{ij}^{(4)}$ by u_{ij}.

Remark. A thorough analysis would contain an estimate of the part of the solution of Eq. (9) that is neglected when the ansatz (10) is considered.

We will now solve the model equation, Eq. (11), analytically for the case $\tan \varphi = 0.5$. Consider Eq. (11) where $a = \cos \theta$, $b = \sin \theta$, with $\theta = \varphi - 90°$, and $\tan \varphi = 0.5$. This two-dimensional difference equation is solved on the domain described in Fig. 3. Boundary conditions are needed at the black points and as $i \to \infty$ and $j \to -\infty$.

We normalize and consider the boundary conditions

$$u_{00} = u_{21} = \cdots = u_{2i,i} = \cdots = 1 \tag{12}$$

$$u_{11} = u_{32} = \cdots = u_{2i-1,i} = \cdots = \beta \tag{13}$$

$$u_{i,j} \to 0, \quad i \to \infty, \quad \text{J} \to -\infty. \tag{14}$$

To solve the difference equation we make the ansatz

$$u_{ij} = \sum_{k=1}^{M} \alpha_k \kappa_k^i \sigma_k^j, \tag{15}$$

where α_k are constants, independent of i and j, and κ_k and σ_k are the roots of the corresponding characteristic equation. Also, M is the number of independent solutions of the characteristic equation.

In the following, we only consider disturbances for which the solution, $u_{i,j}$, is constant in the direction tangential to the shock. That is, $\kappa_k^2 \sigma_k = 1$. Simple algebra yields

LEMMA 2. *The characteristic equation of Eq. (11), together with the condition that $\kappa^2 \sigma = 1$, is*

$$(\kappa - 1)(c_1 \kappa^3 + c_2 \kappa^2 + c_3 \kappa + c_4) = 0 \tag{16}$$

with

$$c_1 = -\frac{\lambda b}{2} - \frac{aU_{//}}{2} - \frac{\varepsilon_y}{h}, \qquad c_2 = \frac{a-b}{2}\lambda - \frac{a+b}{2}U_{//} - \frac{\varepsilon^x + \varepsilon^y}{h}$$

$$c_3 = \frac{a-b}{2}\lambda - \frac{a+b}{2}U_{//} + \frac{\varepsilon^x + \varepsilon^y}{h}, \quad c_4 = -\frac{\lambda b}{2} - \frac{aU_{//}}{2} + \frac{\varepsilon_y}{h},$$

and where $\lambda = U_\perp - C$, $a = \cos\theta$, $b = \sin\theta$, *with* $\theta = \varphi - 90°$ *and* $\tan\varphi = 0.5$.

The boundary condition (14) excludes roots of (16) which are on or outside the unit circle. We therefore proceed to determine the size of the different roots.

The roots of a polynomial with real coefficients vary continuously with the coefficients c_i [18]. We see that $c_1 \neq 0$ for the physical constraints $\varepsilon^y > 0$ and $U_{//} > 0$. Straightforward calculations yield that $\kappa_4 = 1$ is the only root of (16) with $|\kappa| = 1$. With $\lambda = -0.31$, $U_{//} = 1.91$, and $\varepsilon^x = \varepsilon^y = 0.5$ it holds that $|\kappa_{1,2}| < 1$, $|\kappa_3| > 1$, and $|\kappa_4| = 1$. Therefore, since no root can cross the unit circle, we have

LEMMA 3. *For the roots of (16) it holds that*

$$|\kappa_{1,2}| < 1, \quad |\kappa_{3,4}| \geq 1.$$

The boundary conditions (12) and (13) can be written as follows.

LEMMA 4. *The boundary conditions (12) and (13) are equivalent with*

$$\sum_{k=1}^{M} \alpha_k = 1, \sum_{k=1}^{M} \alpha_k \kappa_k \sigma_k = \beta$$

under the constraint that $u_{i,j}$ *is constant tangential to the shock; that is,* $\kappa_k^2 \sigma_k = 1$. M *is the number of independent solutions of (16).*

Proof. The boundary condition (12) can be written as

$$\sum_{k=1}^{M} \alpha_k (\kappa_k^2 \sigma_k)^p = 1, \quad p = 0, 1, \ldots.$$

With $\kappa_k^2 \sigma_k = 1$ then naturally $\sum_{k=1}^{M} \alpha_k (\kappa_k^2 \sigma_k)^p = \sum_{k=1}^{M} \alpha_k$ for $p = 0, 1, \ldots$.

The boundary condition (13) can be written as $\sum_{k=1}^{M} \alpha_k \kappa_k \sigma_k (\kappa_k^2 \sigma_k)^p = \beta$ for $p = 0, 1, \ldots$. With $\kappa_k^2 \sigma_k = 1$, we conclude that $\sum_{k=1}^{M} \alpha_k \kappa_k \sigma_k = \beta$.

With the boundary conditions (12)–(14) we finally have

LEMMA 5. *The solution of the model problem (11), together with boundary conditions (12)–(14) and* $\kappa_k^2 \sigma_k = 1$, *is*

$$u_{ij} = \frac{1 - \beta\kappa_2}{\kappa_1 - \kappa_2} \kappa_1^{1+i-2j} + \frac{\beta\kappa_1 - 1}{\kappa_1 - \kappa_2} \kappa_2^{1+i-2j}, \tag{17}$$

where $\kappa_{1,2}$ *are the roots of the characteristic equation (16) with* $|\kappa_{1,2}| < 1$.

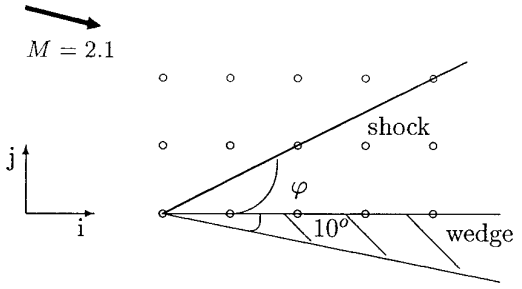

FIG. 4. Computational domain for the oblique shock problem.

Proof. Straightforward calculations yield the lemma.

We repeat that the result in Lemma 5 provides an explicit way to study the solution of the Euler equations downstream of an oblique shock, as a function of ε^x and ε^y.

The same analysis can in principle be made for any φ for which $\tan \varphi$ is a rational number. It is particularly easy for the $\varphi = 45°$ case, since the characteristic equation then becomes quadratic in κ. However, the normal and tangential directions are very well approximated by the central differences in the 45°-case, and hence, that case is more one-dimensional in nature than, e.g. the case $\tan \varphi = 0.5$.

4. NUMERICAL RESULTS

4.1. *Model Equation Compared with the Euler Equations*

In this section we numerically compare the influence of the artificial viscosity terms on the solutions of the Euler equations and the model equation derived in the previous section.

First, we used scheme (4) to solve the two-dimensional Euler equations with initial data to form an oblique shock. We integrated in time with a Runge–Kutta scheme until steady state was reached. The initial data was the inviscid solution for different shock angles. The same steady state solution was obtained for all initial data. The computational domain is described in Fig. 4. The steady state shock angle was $\varphi = 27°$, the upstream Mach number was 2.1 and $M_\perp = 1.7$.

Second, we studied the solution of the model equation, given by (17) and the analogous equation for the upstream problem, with values of a, b, $U_{//}$ and $\lambda = U_\perp - C$, corresponding to the downstream and upstream states of the above oblique shock problem, respectively. The same values of ε^x and ε^y were used in both the model problem and the Euler equations. In the model problem we set $\beta = 1$.

In Fig. 5 we show the solution of the Euler equations for $y = 0.25$ (upper and middle pictures) and the corresponding model equation for the upstream and the downstream state, respectively. For the Euler equations we have chosen to plot the quantity $R_4 = u_\perp - 2c/(\gamma - 1)$. This is the Riemann invariant in the rotated coordinate system that contains the largest jump across the shock. We see that the

same values of ε^x and ε^y for both the model problem and the Euler equations gave the same behavior near the shock.

In Fig. 6 we have plotted the density as a function of x for $y = 0.25$. We see that the density behaves similarly as R_4 that was plotted in Fig. 5.

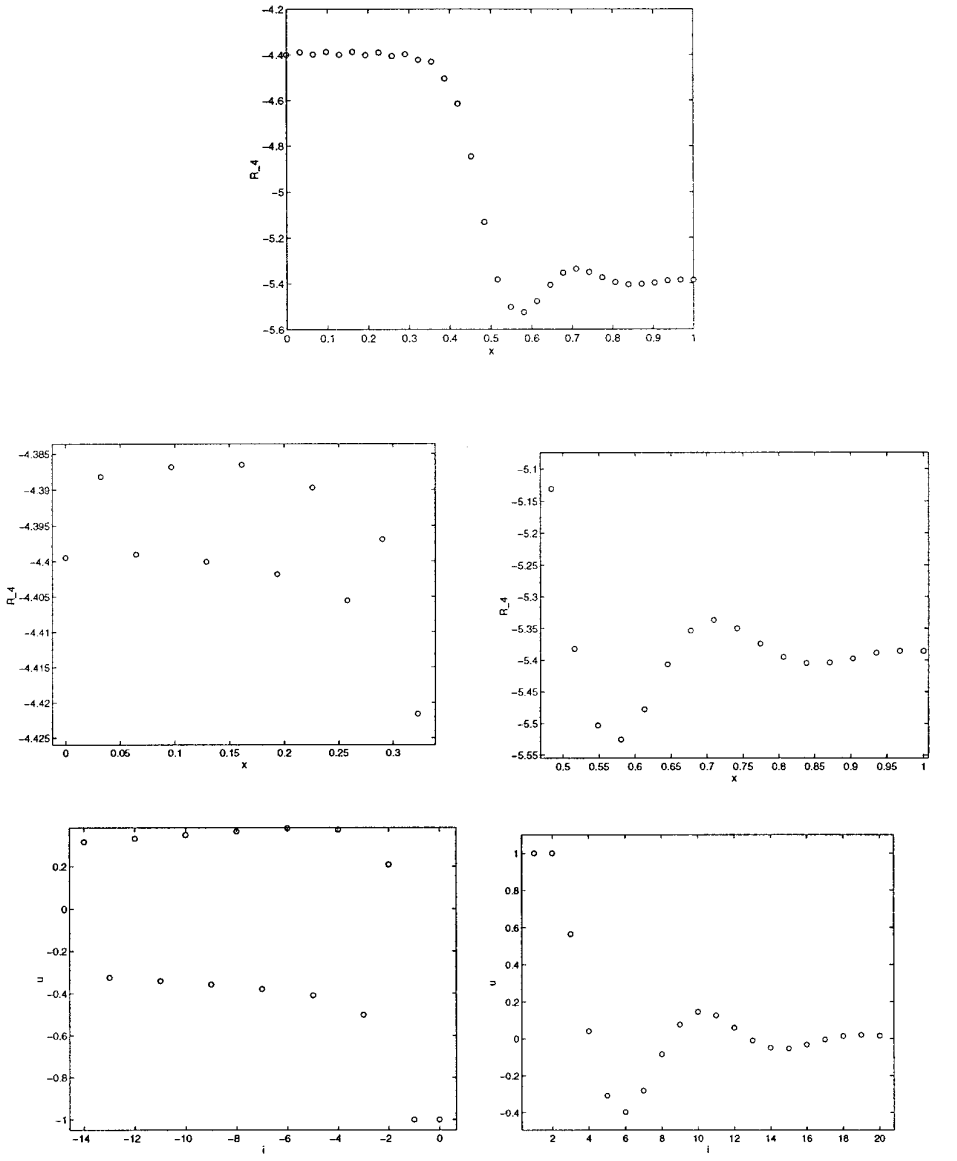

FIG. 5. Comparisons of the solutions of the Euler equations and of the model equations upstream and the downstream state of the shock, respectively. Top: Solution of the Euler equations at $y = 0.25$. $R_4 = u_\perp - 2c/(\gamma - 1)$ as a function of x. $\Delta x = \Delta y = h = 1/30$. $\varepsilon^x = \varepsilon^y = 0.01h$ for $\lambda_{\perp,4} = u_\perp - c > 0$ and $\varepsilon^x = \varepsilon^y = 0.05h$ elsewhere. Middle: Closeup of the solution of the Euler equations for $0 \leq x \leq 0.33$ and $0.5 \leq x \leq 1$, respectively. Bottom: Solution of the model equations corresponding to upstream and downstream of the shock, respectively.

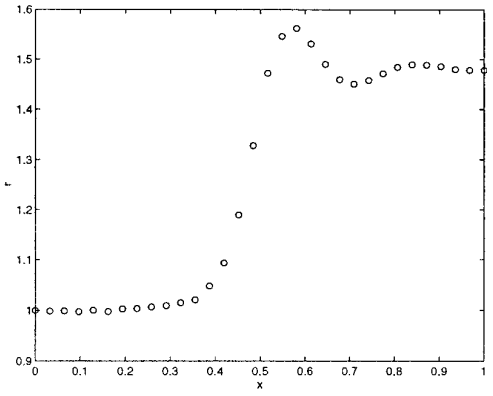

FIG. 6. Density as a function of x for $y = 0.25$. $\Delta x = \Delta y = h = 1/30$. $\varepsilon^x = \varepsilon^y = 0.01h$, where $\lambda_{\perp,4} = u_\perp - c > 0$ and $\varepsilon^x = \varepsilon^y = 0.05h$ elsewhere.

For the Euler equations we used the following boundary conditions. We specified all variables on the top and left boundaries. All variables were extrapolated at the right boundary. In accordance with Davis [4], we used the following conditions at the lower boundary. We set the normal velocity to zero and used the isentropic conditions

$$c - \frac{\gamma - 1}{2} v = \text{const}$$

$$p/p^\gamma = \text{const}$$

to specify the pressure and density at the wall. The tangential velocity was determined from the condition that along the wall the total enthalpy should be constant. This yields

$$\frac{e + p}{p} = \frac{\gamma}{\gamma - 1} p/p + u^2/2 = \text{const}$$

from which u can be determined once p and ρ are known.

4.2. *Development of an Artificial Viscosity Model*

We now use the model equation to determine a suitable numerical viscosity model for a 2D shock. We consider a shock for which the shock angle $\varphi \in [0, \pi/2]$. Then $a > 0$, $b < 0$, where a and b are defined in Lemma 1.

To start, we chose viscosity terms of the form

$$\varepsilon^x = \alpha_1^x(\varphi) g_1^x(\lambda) + \alpha_2^x(\varphi) g_2^x(U_{//}), \quad \varepsilon^y = \alpha_1^y(\varphi) g_1^y(\lambda) + \alpha_2^y(\varphi) g_2^y(U_{//}). \tag{18}$$

First we determined g_1 and g_2 by using the solution of the model problem (17). Thereafter we determined α_1 and α_2 from numerical experiments with the Euler equations.

The solution of the model problem for $\tan \varphi = 0.5$, given by (17) for $\tan \varphi = 0.5$, was studied for different values of λ and $U_{//}$. We wanted to optimize the solution with respect to ε^x and ε^y in the sense that as little smearing as possible was allowed and that the solution should not contain any oscillations. To measure the "well-behaved"-ness we used the weighted discrete 2-norm,

$$\|u\|_{2,h} = \left(\frac{1}{N} \sum_{i=1}^{N} u_i^2 i \right)^{1/2},$$

together with the extra condition that $u_i > 0 \ \forall i$. By a trial-and-error procedure we determined suitable values of ε^x and ε^y for some different $U_{//}$ and λ. From these results we concluded that a good choice was

$$g_1^x = g_1^y = \lambda, \quad g_2^x = g_2^y = U_{//}. \tag{19}$$

Also, we obtained the numerical values of α_1 and α_2 for $\tan \varphi = 0.5$. In order to use (18) for all shock angles, $\varphi \in [0, \pi/2]$, it remained to determine the functions $\alpha_1(\varphi)$ and $\alpha_2(\varphi)$. From numerical experiments with the Euler equations we found that

$$\varepsilon_{i,j}^x = |(a-b)\lambda_{i,j} + b(a+b)(u_{//})_{i,j}|h/2, \quad \varepsilon_{i,j}^y = |(a-b)\lambda_{i,j} + a(a+b)(u_{//})_{i,j}|h/2 \tag{20}$$

gave well-behaved solutions. (See Fig. 7 where three-dimensional pictures of the density for three different shock angles are presented. Note that we only consider shocks with shock angle $\varphi \in [0, \pi/2]$.)

In cases where the shock angle $\varphi \in [\pi/2, 2\pi]$, one can similarly construct artificial viscosity terms of the form (18). However, the numerical viscosity model suggested above is most likely not an optimal one. It can surely be improved to give even better results for the Euler equations. Therefore we found it of less interest to develop the artificial viscosity terms in the same way for $\varphi \in [\pi/2, 2\pi]$. Yet we want to stress that the construction of suitable viscous terms for the model problem gave satisfying results also for the real 2D shock problem.

4.3. *Mach-3 Flow in a Wind Tunnel with a Step*

In order to test our results on a more complicated problem which also contained stronger shocks than the above test case, we solved the Euler equations for the well-known Mach-3 flow in a tunnel with a step.

The solution at time $T = 4$ contains oblique, reflected shocks, a Mach stem, and a contact discontinuity originating from the Mach stem. Computations until $T = 12$ indicate that the structure of the solution can be regarded as stationary. Since we are only interested in the resolution of the shocks we can compare the numerical results at $T = 4$ with our steady state theory. However, at the upper boundary of the step the solution will continue to alter in time, due to the bad resolution of the expansion fan and the solution can, hence, not be regarded as fully stationary.

In Fig. 8 we show the density in a contour plot and for $y = 0.5$. The position of the Mach stem is considered to be in line with the corner of the step. In the figure this position is marked with a straight solid line. Here we used a first-order artificial viscosity term in the whole domain. The left picture is computed with

$$\varepsilon^x_{i,j} = \rho(\mathbf{f}'(\mathbf{u}_{i,j}))h/2, \quad \varepsilon^y_{i,j} = \rho(\mathbf{g}'(\mathbf{u}_{i,j}))h/2, \tag{21}$$

where $\rho(A)$ denotes the spectral radius of A. This is a standard form of artificial viscosity terms, when the one-dimensional theory is applied in a dimensional splitting fashion. In the right picture we have used the shock-aligned viscosity model proposed in (20). We see that the shocks with shock angle $\varphi \in [0, \pi/2]$, have sharpened considerably. Also, shocks with $\varphi \in [\pi/2, 2\pi]$ have become steeper. Reasonably, these shocks are not as sharp as those for which $\varphi \in [0, \pi/2]$. Note also that the artificial viscosity (20) gave well-behaved solutions also for nonweak shocks.

In many calculations so-called limiters are often used to achieve a second-order scheme outside the shock region (see, e.g. [7, 19]). We therefore found it interesting to numerically investigate the influence of a limiter on the previous calculations. In the neighborhood of a shock the first-order artificial viscosity of the form (20) and (21), respectively, was used. In regions where the solution is smooth, or across

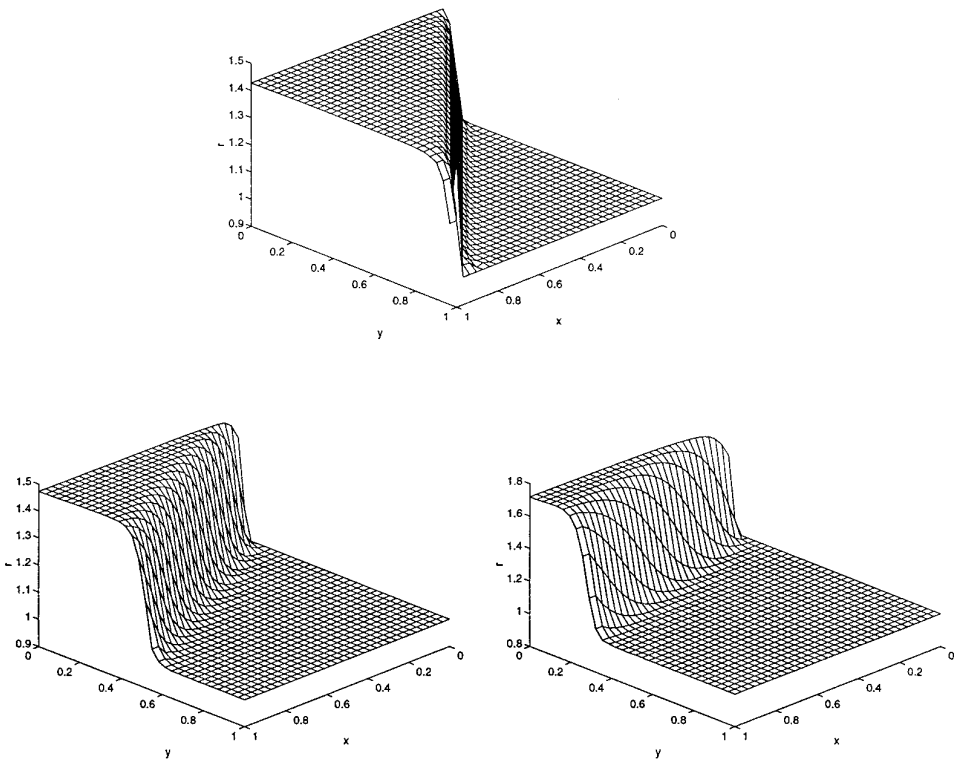

FIG. 7. Density in the oblique shock case (Euler equations). Top: Shock angle 45° $M_\perp = 1.2$; bottom left: shock angle 27° $M_\perp = 1.2$; bottom right: shock angle 15° $M_\perp = 1.4$. $\Delta x = \Delta y = h = 1/30$. ε^x and ε^y chosen as in (20).

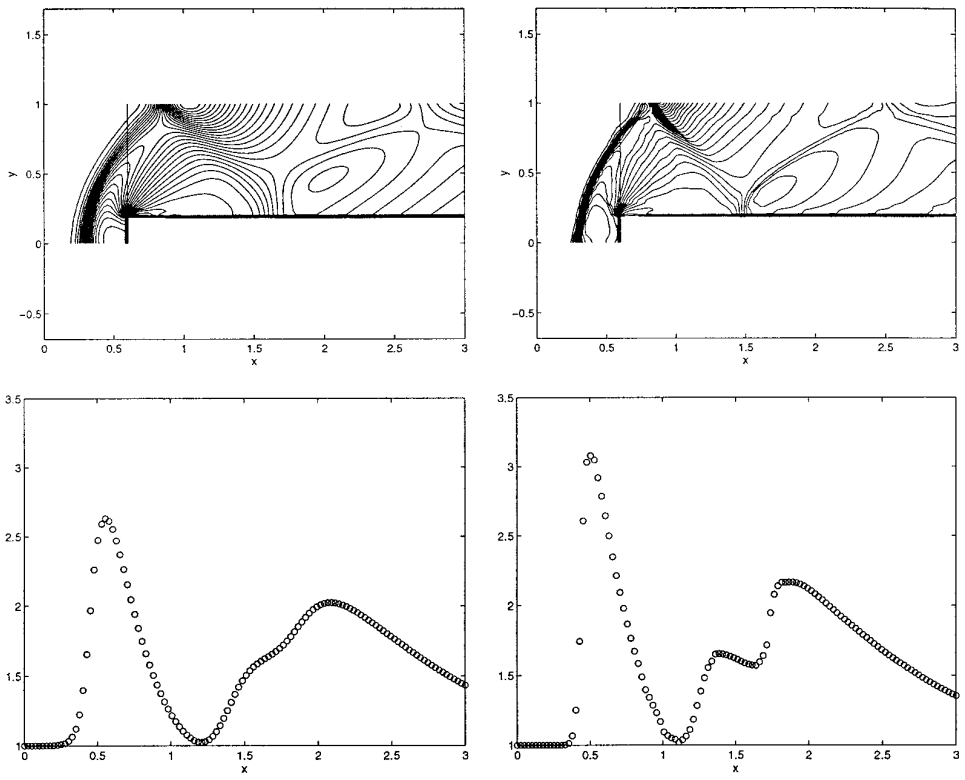

FIG. 8. Density in the Mach 3 flow in a wind tunnel with a step. $\Delta x = \Delta y = h = 1/40$, $T = 4$. No limiter applied. Left: Viscosity terms chosen as in (21). Contour plot and for $y = 0.5$, respectively. Right: Viscosity terms chosen as in (20). Contour plot and for $y = 0.5$, respectively.

a contact discontinuity, a second-order artificial viscosity term, of order $\mathcal{O}(h^2)$, with a fixed value ε_0 was switched on. We applied the so-called minmod-limiter, with the pressure as a limiting variable, as suggested in [7].

It is possible to improve the results of the coordinate aligned scheme even further by applying the switch function to the characteristic variables (see e.g. [7]). This results, however, in a matrix-valued artificial viscosity term.

Contour plots of the density and plots for $y = 0.5$ are shown in Fig. 9 for the two choices of viscosity models, (21) and (20), respectively. We see that in the standard scheme case, the shocks have sharpened considerably. In the case where the artificial viscosity is chosen as in (20), however, the steepness of the shocks is the same as in Fig. 8. Hence, the coordinate-aligned scheme depends heavily on the behavior of the limiter while the scheme with the shock-aligned artificial viscosity is in this sense more insensitive to the limiter.

In the computations above, a fourth-order Runge–Kutta scheme was used to integrate in time. We used a two-block finite-volume solver to compute the solution. Since the grid points were equally distributed and the flux averaging was set to $f_{i+1/2,j} = (f(u_{i,j}) + f(u_{i,j}))/2$ and, accordingly, in the y-direction, this was equivalent to a central difference code, except at the boundaries. We used $\Delta x = \Delta y = h = \frac{1}{40}$ and a time step $\Delta t = \frac{1}{64}$.

Initial data was a uniform gamma-law gas flow with density 1.0, pressure 0.71, velocity 3.0, and $\gamma = 1.4$.

At the inflow boundary, Dirichlet values with the freestream values were used. At the walls we used nonreflecting boundary conditions with linear extrapolation of the pressure. Linear extrapolation of all variables were used at the outflow boundary.

The corner is the center of an expansion fan. Since we do not resolve the solution properly in this region, there will be a boundary layer, a so-called entropy layer, at the wall of the tunnel in the neighborhood of the corner. The reflected shock will interact with the entropy layer and the resulting solution will exhibit unphysical behavior. To damp this error, we apply an extra boundary condition at 10 cells in the corner region, in the sense of Woodward and Colella (see [19]). In these cells we reset the density ρ and the length of the velocity vector U, but not its direction, by solving the nonlinear system

$$\begin{aligned} &\frac{\rho^\gamma}{p(\rho, U)} - \frac{\rho_0^\gamma}{p(\rho_0, U_0)} = 0 && \text{(constant entropy)} \\ &\frac{\gamma}{\gamma - 1}\frac{p(\rho, U)}{\rho} + \frac{U^2}{2} - \frac{\gamma}{\gamma - 1}\frac{p(\rho_0, U_0)}{\rho_0} + \frac{U_0^2}{2} = 0 && \text{(constant enthalpy)} \end{aligned} \tag{22}$$

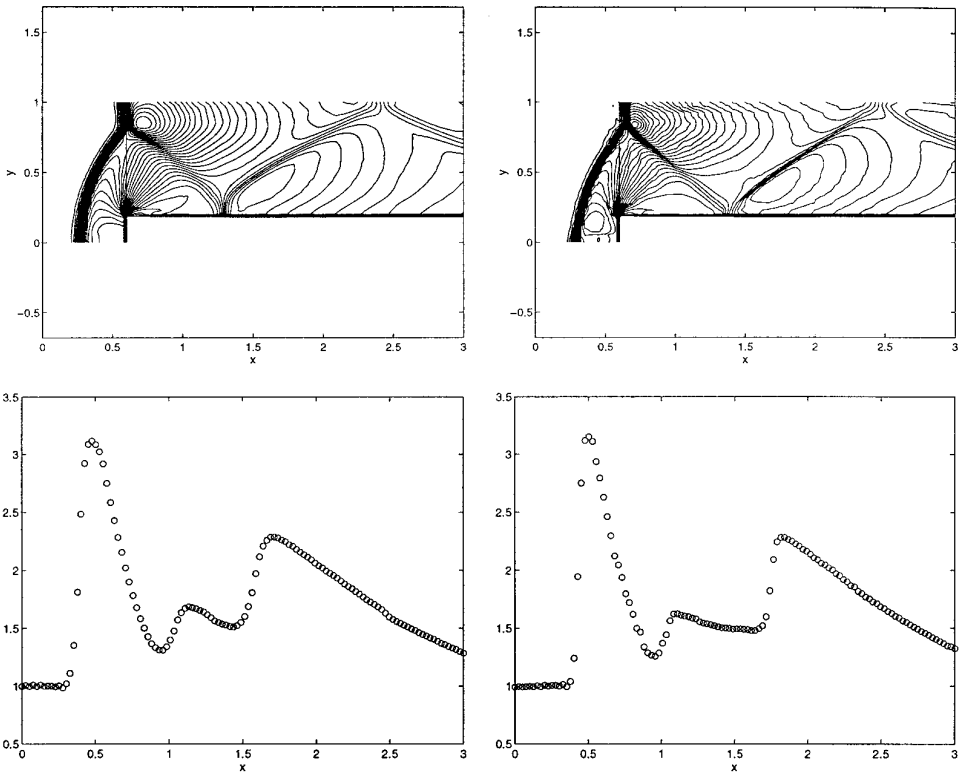

FIG. 9. Density in the Mach-3 flow in a wind tunnel with a step. $\Delta x = \Delta y = 1/40$, $\Delta t = 1/64$, $T = 4$. Minmod limiter with pressure as limiting variable. $\varepsilon_0 = 1.5$. Left: Viscosity terms chosen as in (21). Contour plot and for $y = 0.5$, respectively. Right: Viscosity terms chosen as in (20). Contour plot and for $y = 0.5$, respectively.

with Newton's method. The values ρ_0 and U_0 refer to the values in the cell just to the left and below the corner. This was done in the first six cells in the first row above the corner and in the first four cells in the second row.

Since the shock structure alters in time at the beginning of the calculation, the directions normal to the shocks must be determined during the calculation. In the spirit of Davis [4] we took advantage of the physical rule that the velocity component tangential to the shock, $\mathbf{u}_{//}$, is constant across the shock. Hence,

$$\mathbf{u}_\perp = (u_\perp, v_\perp) = (u, v)_{\text{downstream}} - (u, v)_{\text{upstream}}.$$

Here the indices *downstream* and *upstream* refer to the states downstream and upstream of the shock, respectively. Geometrical considerations now yield that

$$a = u_\perp / \sqrt{u_\perp^2 + v_\perp^2}, \quad b = v_\perp / \sqrt{u_\perp^2 + v_\perp^2},$$

where a and b are the same as in Lemma 1. In general we calculated the normal component as

$$(u_\perp, v_\perp)_{i,j} = (u, v)_{i-1,j} - (u, v)_{i+2,j} := (u_\perp, v_\perp)^x_{i,j}.$$

In this test problem, the shock might be aligned with the x-axis, locally, in the neighborhood of the walls. Therefore, we also computed

$$(u_\perp, v_\perp)^y_{i,j} := (u, v)_{i,j-1} - (u, v)_{i,j+2}$$

and set

$$(u_\perp, v_\perp)_{i,j} = \begin{cases} (u_\perp, v_\perp)^x_{i,j} & \text{if } \|(u_\perp, v_\perp)^x_{i,j}\|_2 > \|(u_\perp, v_\perp)^y_{i,j}\|_2 \\ (u_\perp, v_\perp)^y_{i,j} & \text{otherwise} \end{cases}$$

in the neighborhood of a wall. This was not done in the whole computational domain in order both to stabilize the calculations of $\mathbf{u}_\perp$ and to reduce the amount of work.

We conclude that our numerical viscosity terms, that are a result of studies of a linear scalar problem work well also on a complicated nonlinear problem, together with limiters.

5. CONCLUSIONS

In this article we have presented a way to analyze the influence of artificial viscosity terms in central difference schemes on solutions containing oblique shocks. This is accomplished by solving a linear discrete model equation on a 2D grid. From the solution of the model equation we empirically derive artificial viscosity terms that are two-dimensional in nature.

We try the new artificial viscosity terms on two different test cases: supersonic flow over a wedge and the Mach-3 flow in a wind tunnel with a step. In the latter test case we also study the influence of flux limiters.

We conclude that the study of a linear scalar difference equation gives a comprehensive understanding of the influence of artificial viscosity on the solutions of the two-dimensional Euler equations that contain oblique shocks.

ACKNOWLEDGMENTS

The author thanks Dr. G. Kreiss and Professor H-O. Kreiss for initiating and providing advice throughout the work. The research was funded by the Swedish Research Council for Engineering Sciences (TFR) Grant 92-848.

REFERENCES

1. J. D. Anderson, *Modern Compressible Fluid Flow* (McGraw–Hill, New York, 1990).
2. J. Casper and H. L. Atkins, A finite-volume high-order ENO scheme for two-dimensional hyperbolic systems, *J. Comput. Phys.* **106,** 62 (1993).
3. R. Courant and K. O. Friedrichs, *Supersonic Flow and Shock Waves* (Interscience, New York, 1948).
4. S. F. Davis, A rotational biased upwind difference scheme for the Euler equations, *J. Comput. Phys.* **56,** 65 (1984).
5. H. Deconinck, C. Hirsch, and J. Peuteman, *Characteristic decomposition methods for the multidimensional Euler equations,* in *10th Int. Conf. on Num. Methods in Fluid Dynamics, Beijing, 1986,* p. 216.
6. G. Efraimsson and G. Kreiss, A note on the effect of artificial viscosity on solutions of conservation laws, *Appl. Numer. Math.* **21**(2), 155 (1996).
7. P. Eliasson, *Dissipation Mechanisms and Multigrid Solutions in a Multiblock Solver for Compressible Flow,* Ph.D. thesis, Royal Institute of Technology, Stockholm, Sweden, 1993. [TRITA-NA-R9314, ISSN-0348-2952].
8. J. B. Goodman and R. J. LeVeque, On the accuracy of stable schemes for 2D scalar conservation laws, *Math. Comput.* **45**(171), 15 (1985).
9. A. Harten, High resolution schemes for hyperbolic conservation laws, *J. Comput. Phys.* **49,** 357 (1983).
10. A. Harten, P. D. Lax, and B. van Leer, On upstream differencing and Godunov-type methods for hyperbolic conservation laws, *SIAM Rev.* **25,** 35 (1983).
11. R. J. LeVeque, High resolution finite volume methods on arbitrary grids via wave propagation, *J. Comput. Phys.* **78,** 36 (1988).
12. D. W. Levy, K. G. Powell, and B. van Leer, Use of a rotated Riemann solver for the two-dimensional Euler equations, *J. Comput. Phys.* **106,** 201 (1993).
13. A. Majda, *Compressible Fluid Flow and Systems of Conservation Laws in Several Space Variables* (Springer-Verlag, New York/Berlin, 1984).
14. S. Osher, Riemann solvers, the entropy condition, and difference aproximations, *SIAM J. Numer. Anal.* **21**(2), 217 (1984).
15. P. L. Roe, Discrete models for the numerical analysis of time-dependent multidimensional gas dynamics, *J. Comput. Phys.* **63,** 458 (1986).
16. P. K. Sweby, High resolution schemes using flux limiters for hyperbolic conservation laws, *SIAM J. Numer. Anal.* **21**(5), (1984).
17. E. Tadmor, Numerical viscosity and the entropy condition for conservative difference schemes, *Math. Comp.* **43**(168), 369 (1984).
18. J. H. Wilkinson, *The Algebraic Eigenvalue Problem* (Clarendon Press, Oxford, 1965).
19. P. Woodward and P. Colella, The numerical simulation of two-dimensional fluid flow with strong shocks, *J. Comput. Phys.* **54,** 115 (1984).
20. H. C. Yee, Construction of explicit and implicit symmetric TVD schemes and their application, *J. Comput. Phys.* **68,** 151 (1987).